Energy materials

Facile in-situ fabrication of nanocoral-like bimetallic Co-Mo carbide/nitrogen-doped carbon: a highly active and stable electrocatalyst for hydrogen evolution

Xuejiao Wang[1], Shouxian Chen[1], Pengcheng Zhou[1], Feng Xiao[1], Qihang He[1], Ping He[1,2,*] , Lingpu Jia[1], Bin Jia[2,3], Hui Zhang[2,4], Hongtao Liu[5,*], Kai Pan[6], and Ying Xie[6]

[1] *State Key Laboratory of Environment-Friendly Energy Materials, School of Materials Science and Engineering, Southwest University of Science and Technology, Mianyang 621010, People's Republic of China*

[2] *International Science and Technology Cooperation Laboratory of Micro-Nanoparticle Application Research, Mianyang 621010, People's Republic of China*

[3] *Key Laboratory of Shock and Vibration of Engineering Materials and Structures of Sichuan Province, Southwest University of Science and Technology, Mianyang 621010, People's Republic of China*

[4] *Department of Chemical and Biochemical Engineering, Western University, London, ON N6A 5B9, Canada*

[5] *Hunan Provincial Key Laboratory of Chemical Power Sources, College of Chemistry and Chemical Engineering, Central South University, Changsha 410083, People's Republic of China*

[6] *Key Laboratory of Functional Inorganic Material Chemistry of Ministry of Education, Heilongjiang University, Harbin 150080, People's Republic of China*

ABSTRACT

It is vital to exploit non-noble metal catalysts with ample natural reserve and high performance for reducing energy consumption during electrocatalytic water splitting process. Herein, nanocoral-like bimetallic Co-Mo carbide/nitrogen-doped carbon ($Co-Mo_2C/N-C$) electrocatalysts have been successfully prepared by high temperature pyrolysis of $CoMoO_4$ and melamine for hydrogen evolution reaction (HER). When the mass ratio of $CoMoO_4$ and melamine is 1:15, nanocoral-like $Co-Mo_2C/N-C$ electrocatalyst shows optimal electrocatalytic HER activity, which just needs overpotentials of only 212 and 290 mV at the current density of 10 and 40 mA cm^{-2}, respectively. Besides, it shows low charge transfer resistance and surpassing stability for uninterrupted HER in 1.0 M KOH electrolyte. The eximious electrochemical performance of $Co-Mo_2C/N-C$ is put down to the fact that N-C can effectively disperse $Co-Mo_2C$ nanoparticles. The results suggest that nanocoral-like $Co-Mo_2C/N-C$ with considerable catalytic activity and superior durability is believed as promising candidate to substitute noble metal catalysts for green and renewable hydrogen production by electrocatalytic water splitting.

Handling Editor: Joshua Tong.

Address correspondence to E-mail: heping@swust.edu.cn; liuht@csu.edu.cn

GRAPHICAL ABSTRACT
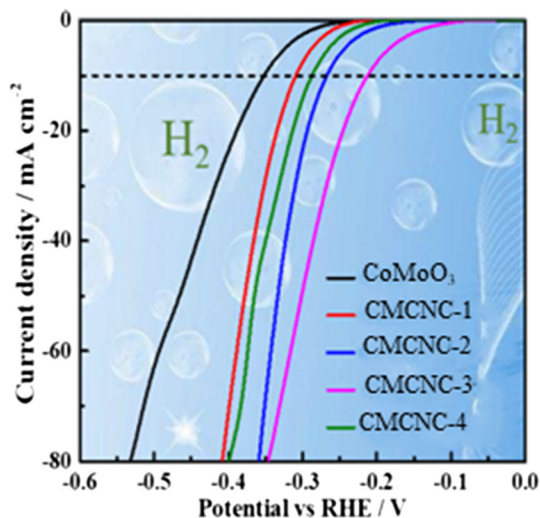
Introduction

With the excessive exhaustion of traditional energy and the deterioration of ecological environment, finding clean and renewable energy with high combustion value has become the urgent demand of human beings [1, 2]. As a promising substitute for traditional energy, hydrogen with recyclability and high energy density has drawn increasing interest [3–5]. With the merits of high efficiency and no environment pollution, electrochemical water splitting is considered as a prospective and reliable technology for hydrogen production [6, 7]. In the process of water splitting, exploiting highly efficient and durable hydrogen evolution reaction (HER) catalysts are critical to reduce the overpotential that brings about excessive energy consumption [8–10]. Though Pt and Pt-based catalysts stick out from various prominent HER catalysts, the fatal drawbacks of exorbitant price and scarce reserves hinder their commercial applications [11]. Thus, the vigorous development of non-precious materials with high activity and stability as HER catalysts is highly imperative [12–14].

Recently, Mo-based catalysts, such as MoS_2 [15], MoN [16], Mo_2C [17], MoB [18] and MoP [19] etc., have been reported with excellent electrocatalytic

HER performance. Among these catalysts, Mo_2C catalyst has attracted extensive attention because of its impressive conductivity, strong corrosion resistance and analogous d-band electronic structure with Pt [20, 21]. Nevertheless, the catalytic performance of Mo_2C is still limited by its inherent shortage of large unoccupied orbitals density and certain aggregation [22, 23]. For reducing the density of unoccupied orbitals of Mo_2C, the design of bimetallic carbide as HER catalysts by adding electron-rich group VIII metal into Mo_2C is an efficient strategy [24]. Hu et al. have reported that $Ni-Mo_2C_{CB}/CFP$ electrocatalysts need overpotential of 121.4 mV at 10 mA cm^{-2} [25]. Lin et al. have prepared Fe_3C-Mo_2C/NC as HER electrocatalysts with overpotential of 116 mV at 10 mA cm^{-2} [26].

As well known, the intimate conjugation between Mo_2C and carbonaceous materials promotes the electrons transport, stabilizes the overall structure, reduces hydrogen Gibbs adsorption free energy of Mo_2C to optimize the absorption of H* and inhibits the aggregation of Mo_2C nanoparticles to some extent, which is propitious to enhance electrocatalytic ability of catalysts [27–29]. Heteroatoms doping, especially nitrogen atoms, can further enhance the electrochemical performance by optimizing the electronic structure of carbon materials [30]. Among carbon materials, nitrogen-doped carbon fabricated

by high temperature pyrolysis of melamine has sparked significant interest for its impressing conductivity, low cost and simple preparation [31]. To the best of our knowledge, there are few reports concerning the application of bimetallic Co-Mo carbide compounding with nitrogen-doped carbon as HER electrocatalysts. Taking these virtues into account, we anticipate that bimetallic Co-Mo carbide/nitrogen-doped carbon (Co-Mo$_2$C/N-C) can serve as HER catalysts with low overpotential.

Herein, nanocoral-like Co-Mo$_2$C/N–C electrocatalyst has been in-situ synthesized by high temperature pyrolysis of CoMoO$_4$ and melamine. As a result, nanocoral-like CMCNC-3 catalyst only needs low overpotentials of 212 and 290 mV at the current density of 10 and 40 mA cm^{-2}, respectively. In addition, CMCNC-3 catalyst shows favorable stability during durative hydrogen generation. The strategy to fabricate efficient and stable Co-Mo$_2$C/-C catalyst offers a broad perspective for the exploitation of metal-carbide-based catalysts toward HER.

Experimental

Chemicals and materials

Na$_2$MoO$_4$ 2H$_2$O, Co(NO$_3$)$_2$ 6H$_2$O, NaOH, melamine, isopropanol and ethanol were obtained from Jiangsu Yatai Chemical Co., Ltd. (Jiangsu, China). Nafion solution (5 wt%) was provided by Sigma-Aldrich (St Louis, USA).

Fabrication of Co-Mo$_2$C/N-C materials

Scheme 1 presented the fabrication procedure for Co-Mo$_2$C/N-C materials. In the first step, as-obtained CoMoO$_4$ precursor was fabricated via hydrothermal method. In detail, 2.0 mmol Na$_2$MoO$_4$ 2H$_2$O and 2.0 mmol Co(NO$_3$)$_2$ 6H$_2$O were added into 40 mL distilled water with stirring for 15 min. Next, the mixture was transferred into Teflon-lined autoclave for hydrothermal treatment at 160 °C for 6 h. The precipitate was washed several times with deionized water and ethanol, and finally dried at 60 °C overnight.

In the second step, Co-Mo$_2$C/N-C materials were fabricated via high temperature pyrolysis of CoMoO$_4$ and melamine. In detail, 100 mg as-fabricated CoMoO$_4$ precursor and a certain mass of melamine were fully mixed by grinding in an agate mortar. Subsequently, the mixture above was transferred into a tube furnace for pyrolysis at 850 °C for 3 h with a heating rate of 5 °C min^{-1} in an argon atmosphere. After pyrolysis, collected product was ground and packaged to be used. The mass ratios between CoMoO$_4$ and melamine were 1:5, 1:10, 1:15 and 1:20, and the corresponding samples were named as CMCNC-1, CMCNC-2, CMCNC-3 and CMCNC-4, respectively.

For comparison, CoMoO$_3$ was fabricated following the steps above without melamine.

Materials characterizations

Scanning electron microscope (SEM, Sigma 300, Carl Zeiss SMT Pte Ltd., Germany) was operated to analyse the morphology. In order to investigate the structure of carbon components, Raman spectrometer (inVia, Renishaw Instrument Co., Britain) was employed. To study the crystal structures of as-fabricated materials, X-ray diffraction (XRD) tests were performed on X' Pert PRO diffractometer (PANalytical, Netherlands) using Cu K_α radiation (λ = 0.154060 nm). X-ray photoelectron spectroscope (XPS) tests were conducted on 5000 Versaprobe-II photoelectron spectroscope (ULVAC-PHI, Japan) with Al $K\alpha$ (hυ = 1486.6 eV) to investigate the surface chemical states of materials.
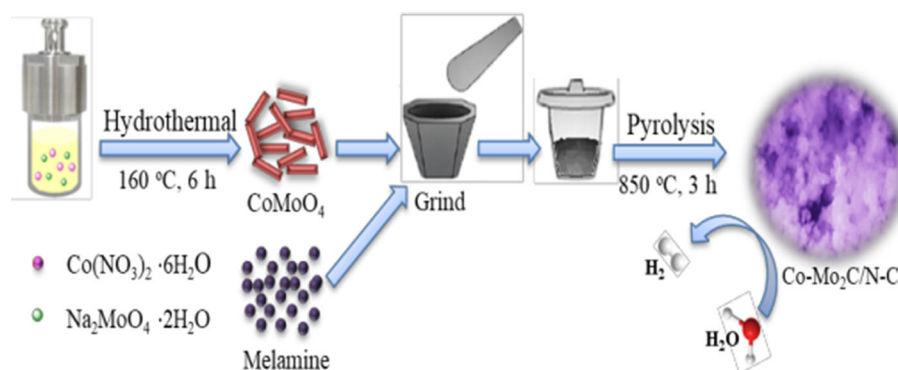
Electrode fabrication and electrochemical measurements

Fabrication of working electrodes

Before use, glassy carbon electrode was polished on chamois leather using aluminum oxide powders and washed thoroughly with ethanol and distilled water and finally dried naturally.

As-fabricated active materials (5.0 mg) were ultrasonically dispersed in 1.0 mL of isopropanol/water ($V_{isopropanol}/V_{water}$ = 3:7) containing 5.0 μL Nafion solution (5 wt%) to form homogeneous material ink. Next, the ink above (5.0 μL) was dripped onto GCE, and finally dried at ambient environment. The mass loading of material on GCE was about 0.35 mg cm^{-2}.

Scheme 1 Fabrication procedure for Co–Mo$_2$C/N-C materials.

Electrochemical measurements of as-fabricated materials

Polarization curves, electrochemical impedance spectroscopy (EIS) and cyclic voltammetry (CV) were operated on PARSTAT 2273 electrochemical workstation (Princeton Applied Research, USA), and chronoamperometry measurements were conducted on DH7000 electrochemical workstation (Jiangsu Donghua Analysis Instrument Co., Ltd., Jingjiang, China) in 1.0 M KOH solution at ambient environment with a standard three-electrode system. Reference electrode, working electrode and counter electrode were HgO/Hg electrode, as-fabricated electrode and graphite rod, respectively. In this work, all potentials measured were obtained after IR correction and converted to reversible hydrogen electrode (RHE) according to the following formula: $E_{RHE} = (E_{HgO/Hg} + 0.098 \text{ V}) + 0.059 \text{ pH}$. Before the electrochemical measurements, all 1.0 M KOH electrolytes were saturated with N$_2$ for 1 h.

Results and discussion

Characterizations of structure, component and morphology

Shown in Fig. 1 is the Raman spectrum of CMCNC-3 catalyst. Two peaks at 1317.2 and 1590.4 cm^{-1} are ascribed to D and G bands, respectively, confirming the presence of disordered carbon and graphitic carbon in CMCNC-3 [32]. In addition, the calculated intensity ratio of D band and G band value for CMCNC-3 is 1.4, verifying that it possesses low graphitized degree and a large number of structural defects [33].

XRD tests are carried out to study crystal structure of CoMoO$_4$ (a), CoMoO$_3$ (b) and CMCNC-3
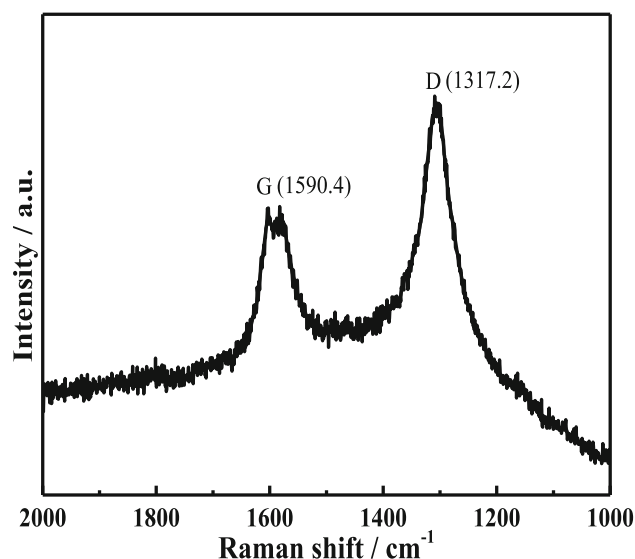

Figure 1 Raman spectrum of CMCNC-3 catalyst.

(c) (Fig. 2). As for CoMoO$_4$ (curve a), the peaks at 13.4°, 23.2°, 26.9°, 29.3°, 34.3° and 52.8° correspond to (001), (021), (002), (310), (022) and (440) crystal planes of CoMoO$_4$ (JCPDS 21–0868) [34], respectively. As for CoMoO$_3$ (curve b), the peaks at 18.0°, 25.4°, 32.7°, 36.1°, 37.2°, 40.5°, 45.5°, 49.2°, 52.1°, 56.2°, 59.8°, 62.5° and 64.6° are ascribed to (002), (102), (103), (200), (004), (104), (203), (114), (204), (006), (205), (303) and (220) crystal planes of CoMoO$_3$ (JCPDS 21-0869) [35], respectively. As for CMCNC-3 (curve c), a peak at 26.5° is typical (002) crystal plane of graphitic carbon [36]. The peaks at 36.1°, 51.9°, 64.6°, 73.9° and 76.1° are ascribed to (100), (102), (110), (112) and (201) crystal planes of β-Mo$_2$C (JCPDS 35–0787) [37]. The peaks at 32.1°, 44.5° and 49.1° are ascribed to (400), (511) and (442) crystal planes of Mo$_3$Co$_3$C (JCPDS 65-7128) [38]. The results prove the coexistence of β-Mo$_2$C, Mo$_3$Co$_3$C and graphitic carbon in CMCNC-3.
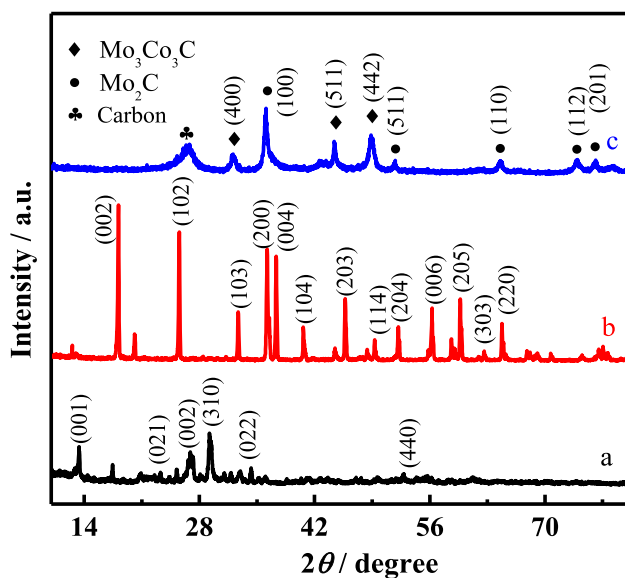
Figure 2 XRD patterns of CoMoO$_4$ **a**, CoMoO$_3$ **b** and CMCNC-3 **c**.

The surface electronic states of CoMoO$_4$, CoMoO$_3$ and CMCNC-3 catalysts are investigated by XPS analyses (Fig. 3). In Fig. 3a, Co 2p spectrum of CoMoO$_4$ exhibits five peaks at 780.9, 782.1, 787.1, 797.5 and 803.2 eV. Two peaks at 780.9 and 782.1 eV belong to Co 2p$_{3/2}$, and a peak at 797.5 eV belongs to Co 2p$_{1/2}$ [39, 40]. In addition, two peaks at 787.1 and 803.2 eV belong to satellite peaks [41]. Mo 3d spectrum of CoMoO$_4$ (Fig. 3b) shows two peaks at 231.9 and 235.1 eV, which correspond to Mo 2d$_{5/2}$ and Mo 2d$_{3/2}$, respectively [42, 43]. In O 1 s spectrum of CoMoO$_4$ (Fig. 3c), a peak at 530.7 eV is related to lattice oxygen, while a peak at 533.2 eV is attributed to –OH on the surface of CoMoO$_4$ [44].

In Fig. 3d, Co 2p spectrum of CoMoO$_3$ shows two peaks at 781.9 and 797.4 eV, which belong to Co 2p$_{3/2}$ and Co 2p$_{1/2}$, respectively. Additionally, two peaks at 786.4 and 804.3 eV correspond to shake-up satellite peaks [45]. In Mo 3d spectrum of CoMoO$_3$ (Fig. 3e), two peaks at 229.9 and 233.0 eV belong to Mo^{4+}, while two peaks at 231.7 and 234.7 eV are assigned to Mo^{6+} [46]. In Fig. 3f, O 1s spectrum of CoMoO$_3$ displays two peaks at 530.6 and 532.3 eV, which belong to lattice oxygen and –OH on the surface of CoMoO$_3$, respectively [47].

Co 2p spectrum of CMCNC-3 (Fig. 3g) exhibits the peaks at 781.7 and 797.9 eV, which are assigned to Co^{2+} [48]. In addition, two peaks at 783.9 and 799.4 eV are assigned to Co^{3+} [49]. The peaks at 787.6,

803.7 and 805.8 eV correspond to satellite peaks [50]. As displayed in Fig. 3h, Mo 3d spectrum of CMCNC-3 exhibits six peaks at 228.4, 229.2, 231.6, 232.3, 232.9 and 235.6 eV. Two peaks at 228.4 and 231.6 eV are attributed to Mo-C [51]. Two peaks at 229.2 and 232.9 eV belong to Mo^{4+}, while two peaks at 232.3 and 235.6 eV belong to Mo^{6+} [52]. In C 1 s spectrum of CMCNC-3 (Fig. 3i), two peaks at 284.8 and 286.0 eV belong to C–C/C = C and C-N bond, respectively [53]. In Fig. 3j, N 1s spectrum of CMCNC-3 shows the peaks at 394.2, 397.7, 398.5 and 400.3 eV, which belong to Mo–N, pyridinic-N, pyrrolic-N and graphitic-N, respectively [54, 55].

SEM images of CoMoO$_4$, CoMoO$_3$ and CMCNC-3 are shown in Fig. 4a ∼ c. CoMoO$_4$ (Fig. 4a) displays uneven nanorods morphology with certain agglomeration. CoMoO$_3$ (Fig. 4b) shows nanocoral-like morphology. However, its nonuniform and aggregation impede the exposure of active sites to a certain degree. After the addition of melamine in the precursor, CMCNC-3 catalyst (Fig. 4c) exhibits looser nanocoral-like morphology assembled by numerous more uniform nanoparticles in comparison with CoMoO$_3$, exposing enough electrocatalytic active sites. EDS elemental mapping images of CMCNC-3 are exhibited in Fig. 4e∼h, demonstrating that four elements (Co, Mo, C and N) are uniformly dispersed in CMCNC-3.

Electrochemical characterizations

Polarization curves of as-fabricated electrocatalysts with a scan rate of 1 mV s^{-1} using a three-electrode system in 1.0 M KOH electrolyte are presented in Fig. 5a. Co-Mo$_2$C/N–C catalyst displays improved electrocatalytic performance with lower overpotential toward HER in comparison with CoMoO$_3$. Additionally, CMCNC-3 catalyst exhibits better electrocatalytic activity with onset potential as low as 106 mV, while 257 mV, 237 mV, 175 mV and 221 mV for CoMoO$_3$, CMCNC-1, CMCNC-2 and CMCNC-4, respectively. Clearly, CMCNC-3 catalyst manifests lower overpotential (212 mV) than those of CoMoO$_3$ (352 mV), CMCNC-1 (309 mV), CMCNC-2 (267 mV) and CMCNC-4 (288 mV) at 10 mA cm^{-2}. CMCNC-3 catalyst displays an overpotential of 290 mV at 40 mA cm^{-2}, which is lower than CoMoO$_3$ (440 mV), CMCNC-1 (366 mV), CMCNC-2 (323 mV) and CMCNC-4 (350 mV).

Figure 3 XPS spectra of CoMoO$_4$ **a–c**, CoMoO$_3$ **d–f** and CMCNC-3 **g–j**.
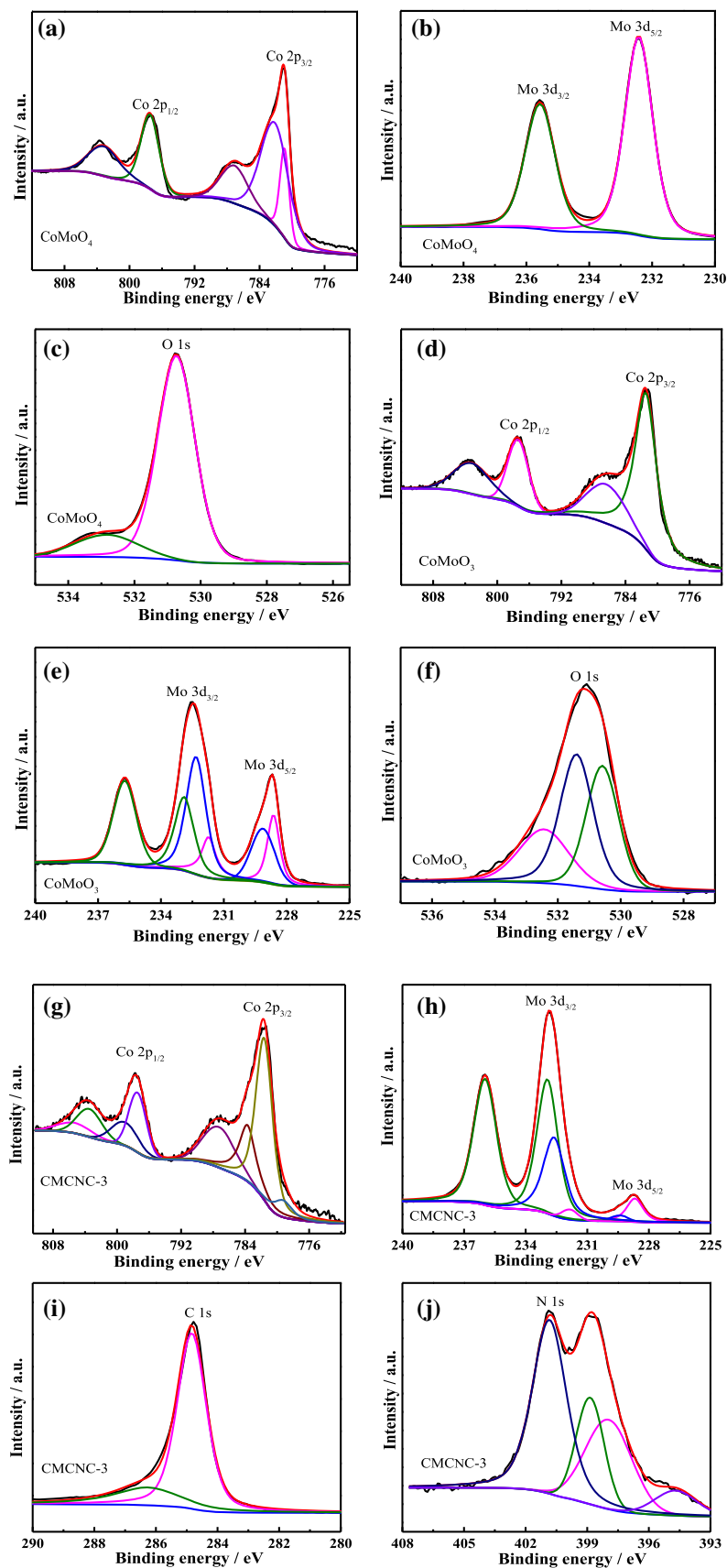
Figure 4 SEM images of CoMoO$_4$ **a**, CoMoO$_3$ **b** and CMCNC-3 catalysts **c**; SEM image **d** and EDS elemental mappings **e–h** of CMCNC-3 catalyst.
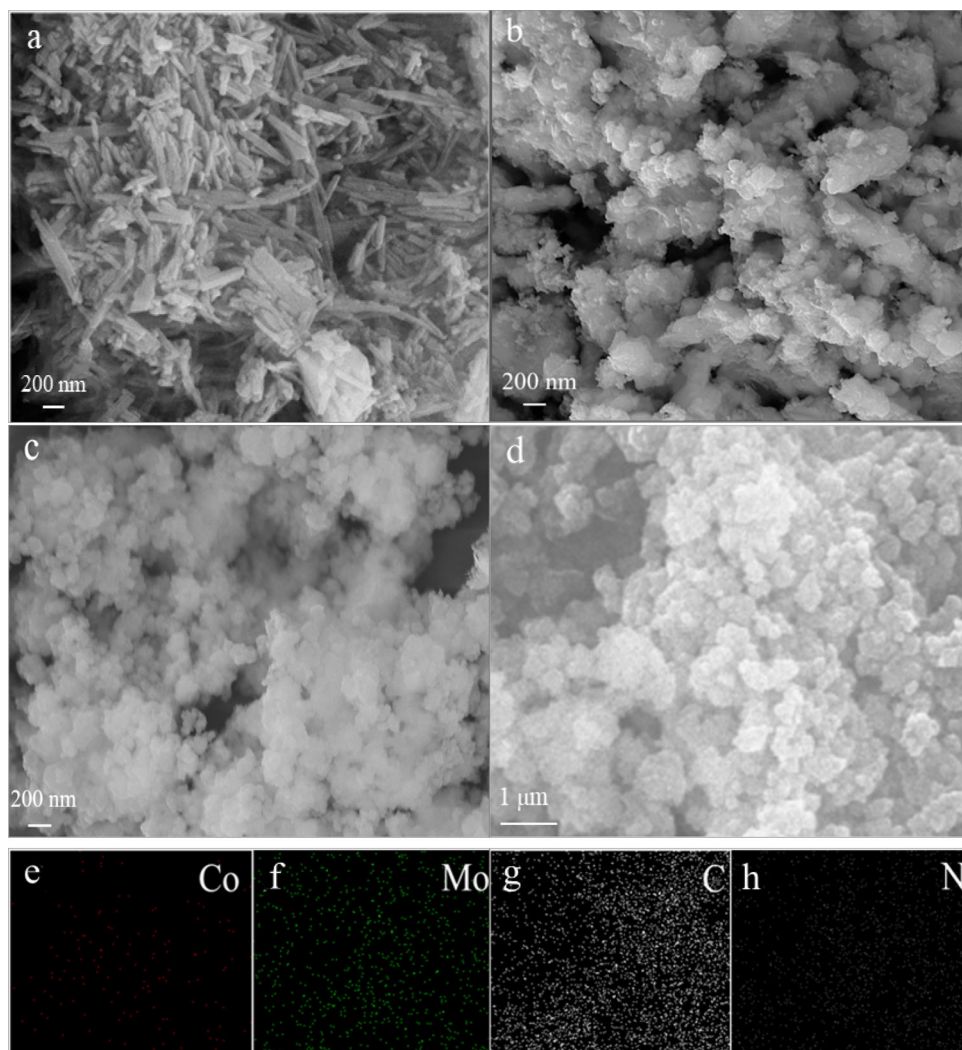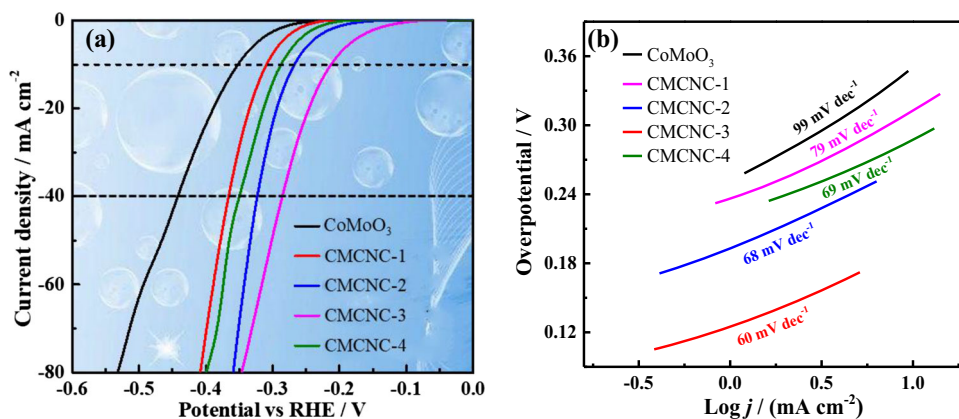

Figure 5 Polarization curves (**a**) and corresponding Tafel plots (**b**) of CoMoO$_3$, CMCNC-1, CMCNC-2, CMCNC-3 and CMCNC-4 catalysts.


Co-Mo$_2$C/N-C catalyst has looser structure than CoMoO$_3$, which exposes more catalytic active sites, leading to excellent catalytic activity toward HER. Besides, owing to the synergistic effect between Mo$_2$C, Mo$_3$Co$_3$C and N–C, CMCNC-3 catalyst shows commendable HER activity.

In Fig. 5b, Tafel plots are used to study the HER kinetics of as-fabricated catalysts. Tafel slope is

Figure 6 CV curves of
$CoMoO_3$ (**a**), CMCNC-1 (**b**),
CMCNC-2 (**c**), CMCNC-3
(**d**) and CMCNC-4 catalysts
(**e**) under different scan rates;
plots of the capacitive currents
as a function of scan rates (**f**).
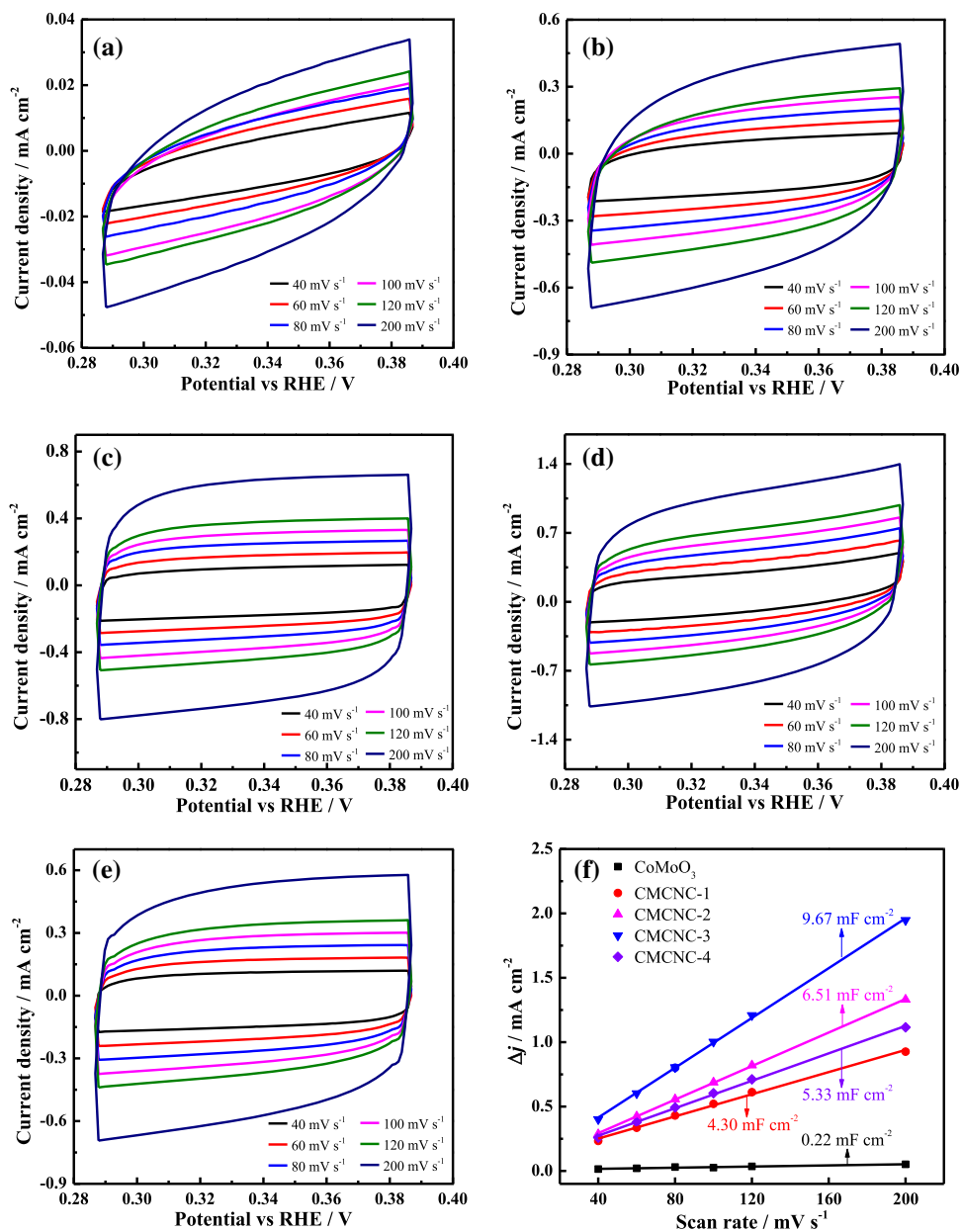
calculated by Tafel equations as follows:
$\eta = a + b \log j$, where η is overpotential, a the constant, b the Tafel slope (mV dec^{-1}) and j the current density (mA cm^{-2}) [6]. As observed, $CoMoO_3$, CMCNC-1, CMCNC-2, CMCNC-3 and CMCNC-4 catalysts show Tafel slope values of 99, 79, 68, 60 and 69 mV dec^{-1}, respectively. Obviously, CMCNC-3 catalyst manifests smaller value of Tafel slope than other four catalysts, suggesting faster kinetics for electrocatalytic HER, which contributes to rapid reaction on its surfaces. In addition, Tafel slopes of 118, 40 and 30 mV dec^{-1} correspond to Volmer, Heyrovsky and Tafel reaction during HER process in

alkaline solutions, respectively [56, 57]. The results indicate that rate-limiting mechanism of as-fabricated catalysts is Volmer-Heyrovsky mechanism.

To further investigate HER electrocatalytic performance of $CoMoO_3$, CMCNC-1, CMCNC-2, CMCNC-3 and CMCNC-4, the electrochemically active surface areas (ECSA) are assessed by electrochemical double-layer capacitance (C_{dl}). In Fig. 6a $\sim$ e, CV tests of as-fabricated catalysts are carried out in non-Faradaic potential region (0.290 V $\sim$ 0.390 V vs. RHE) with diverse scan rates (40 mV s^{-1} $\sim$ 200 mV s^{-1}). As shown in Fig. 6f, current density Δj (j_{anode}—$j_{cathode}$) at 0.34 V vs. RHE against scan rate shows the linear
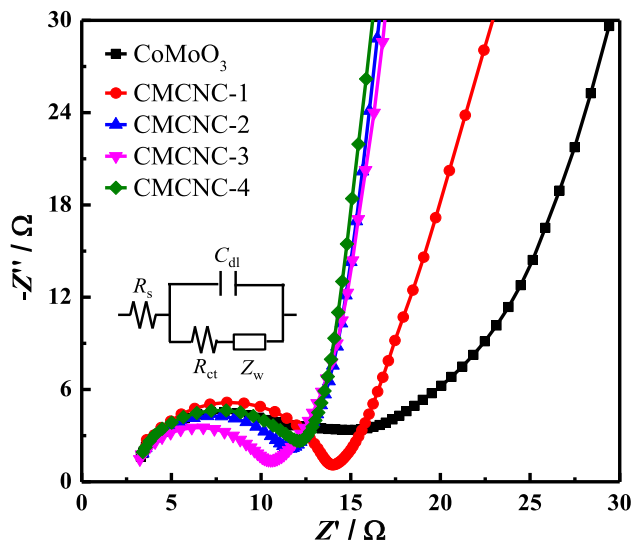
Figure 7 Nyquist plots of CoMoO$_3$, CMCNC-1, CMCNC-2, CMCNC-3 and CMCNC-4 catalysts.

Table 1 Fitted values of equivalent circuit elements based on impedance spectra of as-fabricated catalysts

Catalysts	R_s/Ω	C_{dl}/μF	R_{ct}/Ω	$Z_w \times 10^3$/(S-sec^.5)
CoMoO$_3$	2.95	0.069	9.96	3.88
CMCNC-1	3.16	0.106	9.61	1.54
CMCNC-2	2.79	0.079	7.37	1.15
CMCNC-3	2.85	0.106	6.59	2.56
CMCNC-4	2.75	0.078	7.80	0.88

relationship. Meanwhile, it is clear that C_{dl} value of CMCNC-3 (9.67 mF cm^{-2}) is higher than those of CoMoO$_3$ (0.22 mF cm^{-2}), CMCNC-1 (4.30 mF cm^{-2}), CMCNC-2(6.51 mF cm^{-2}), CMCNC-4 (5.33 mF cm^{-2}), indicating higher ECSA and numerous exposed active sites of CMCNC-3. The high electrocatalytic activity of catalysts is positively related to the enhancement of ECSA and active sites [58]. Thus, nanocoral-like CMCNC-3 catalyst exhibits better HER electrocatalytic performance than all other as-fabricated catalysts.

EIS tests are carried out in the range of $10^6 \sim 10^{-1}$ Hz at open circuit potential with a modulation amplitude of 5 mV, and Nyquist plots are displayed in Fig. 7. In equivalent circuit diagram (the insert in Fig. 7), R_s is the uncompensated solution resistance, R_{ct} is the charge transfer resistance, C_{dl} is the double-layer capacitance, and Z_w is the Warburg impedance. Furthermore, CoMoO$_3$, CMCNC-1, CMCNC-2, CMCNC-3 and CMCNC-4 catalysts show R_{ct} values (Table 1) of 9.96, 9.61, 7.37, 6.59 and 7.80 Ω,
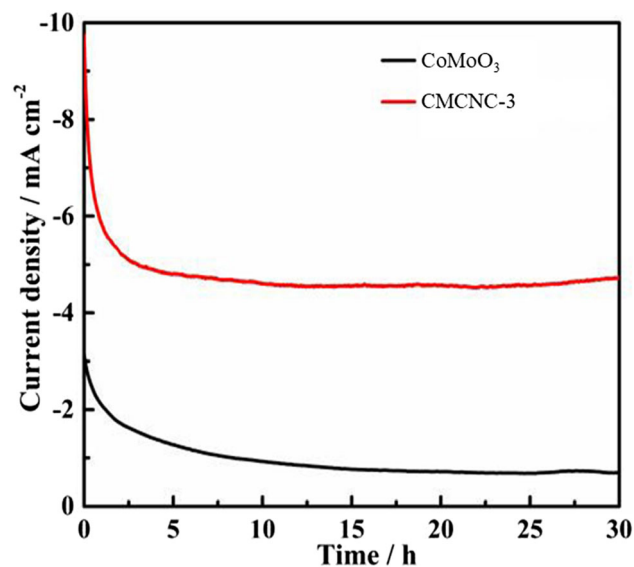

Figure 8 Chronoamperometry tests of CoMoO$_3$ and CMCNC-3 catalysts at overpotential of 212 mV for 30 h.

respectively. The lower R_{ct} value of CMCNC-3 indicates faster electron transfer process.

As shown in Fig. 8, chronoamperometry tests of CoMoO$_3$ and CMCNC-3 catalysts are performed at overpotential of 212 mV in 1.0 M KOH electrolyte. CMCNC-3 catalyst exhibits higher current density than that of CoMoO$_3$ catalyst, indicating that CMCNC-3 catalyst has better HER catalytic activity. In addition, the current density of CMCNC-3 catalyst decreases at firstly and then maintains steady relatively during continuous hydrogen generation, demonstrating eminent long-term durability of CMCNC-3. The favorable HER electrocatalytic activity and stability of CMCNC-3 are ascribed to some reasons as follows: (1) the addition of N-C produced by pyrolysis of melamine, which increases the surface activity and conductivity in theory; (2) the loose nanocoral-like structure assembled by uniform nanoparticles, which provides larger ECSA and abundant ions transport channel; (3) the synergistic effect between Mo$_2$C, Mo$_3$Co$_3$C and N-C.

Conclusions

In summary, Co-Mo$_2$C/N-C catalyst has been in-situ synthesized by high temperature pyrolysis of CoMoO$_4$ and melamine. The nanocoral-like CMCNC-3 needs overpotentials of only 212 and 290 mV at the current density of 10 and 40 mA cm^{-2}, respectively.

Besides, CMCNC-3 shows low charge transfer resistance and outstanding stability during continuous hydrogen generation. The high catalytic activity of CMCNC-3 originates from the efficient dispersion of Co-Mo$_2$C nanoparticles by N-C and the synergistic effect between Mo$_2$C, Mo$_3$Co$_3$C and N-C. The results suggest that nanocoral-like Co-Mo$_2$C/N-C with excellent activity and long-term durability is promising in renewable energy conversion system to achieve massive hydrogen generation.

Declarations

Conflict of interest The authors declare that they have no known competing financial interests or personal relationships in this paper.

References

[1] Liu HH, He P, Jia LP, He MQ, Zhang XQ, Wang S, Zhang XJ, Li CX, Zhang Y, Dong FQ (2018) Cobalt disulfide nanosphere dispersed on multi-walled carbon nanotubes: an efficient and stable electrocatalyst for hydrogen evolution reaction. Ionics 24:3591–3599. https://doi.org/10.1007/s11581-018-2474-x

[2] Liu HH, Lei J, Yang S, Qin F, Cui L, Kong Y, Zheng X, Duan T, Zhu W, He R (2021) Boosting the oxygen evolution activity over cobalt nitride nanosheets through optimizing the electronic configuration. Appl Catal B Environ 286:119894. https://doi.org/10.1016/j.apcatb.2021.119894

[3] Xiong TL, Jia J, Wei ZQ, Zeng LL, Deng YQ, Zhou WJ, Chen SW (2019) N-doped carbon-wrapped Mo$_x$C

[4] Zhang LH, Zhao HT, Xu SR, Liu Q, Li TS, Luo YL, Gao SY, Shi XF, Asiri AM, Sun XP (2020) Recent advances in one-dimensional electrospun nanocatalystsfor electrochemical water splitting. Small Struct. 2:2000048. https://doi.org/10.1002/sstr.202000048

[5] Lu WB, Liu TT, Xie LS, Tang C, Liu DN, Hao S, Qu FL, Du G, Ma YJ, Asiri AM, Sun XP (2017) In situ derived Co-B nanoarray: a high-efficiency and durable 3D bifunctional electrocatalyst for overall alkaline water splitting. Small 13:1700805. https://doi.org/10.1002/smll.201700805

[6] Kong FH, Sun LP, Huo LH, Zhao H (2019) In-situ electrochemical self-tuning of amorphous nickel molybdenum phosphate to crystal Ni-rich compound for enhanced overall water splitting. J Power Sources 430:218–227. https://doi.org/10.1016/j.jpowsour.2019.05.037

[7] Wang XJ, Zhou LH, Yang TT, Gao J, He P, Jia LP, Dong FQ, Jia B, Zhang H (2020) Facile one-step synthesis of tunable nanochain-like Fe-Mo-B: a highly efficient and stable catalyst for oxygen evolution reaction. J Alloy Compd 822:153517. https://doi.org/10.1016/j.jallcom.2019.153517

[8] Jiang JB, Zhu LY, Sun YX, Chen YK, Chen HT, Han S, Lin HL (2019) Fe$_2$O$_3$ nanocatalysts on N-doped carbon nanomaterial for highly efficient electrochemical hydrogen evolution in alkaline. J Power Sources 426:74–83. https://doi.org/10.1016/j.jpowsour.2019.04.022

[9] Zhang WH, Tang YH, Yu LM, Yu XY (2020) Activating the alkaline hydrogen evolution performance of Mo-incorporated Ni(OH)(2) by plasma-induced heterostructure. Appl Catal B Environ 260:118154. https://doi.org/10.1016/j.apcatb.2019.118154

[10] Liu DN, Liu TT, Zhang LX, Qu FL, Du G, Asiri AM, Sun XP (2017) High-performance urea electrolysis towards less energy-intensive electrochemical hydrogen production using a bifunctional catalyst electrode. J Mater Chem A 5:3208–3213. https://doi.org/10.1039/C6TA11127K

[11] Liu HH, Zeng S, He P, Dong FQ, He MQ, Zhang Y, Wang S, Li CX, Liu MZ, Jia LP (2019) Samarium oxide modified Ni-Co nanosheets based three-dimensional honeycomb film on nickel foam: a highly efficient electrocatalyst for hydrogen evolution reaction. Electrochim Acta 299:405–414. https://doi.org/10.1016/j.electacta.2018.12.169

[12] Wu C, Yang YJ, Dong D, Zhang YH, Li JH (2017) In situ coupling of CoP polyhedrons and carbon nanotubes as highly efficient hydrogen evolution reaction electrocatalyst. Small 13:1602873. https://doi.org/10.1002/smll.201602873

[13] Wang Q, Wang ZY, Zhao Y, Li FM, Xu L, Wang XM, Jiao H, Chen Y (2020) Self-supported FeP-CoMoP hierarchical

nanostructures for efficient hydrogen evolution. Chem Asian J 15:1590–1597. https://doi.org/10.1002/asia.202000278

[14] Lin F, Dong ZH, Yao YH, Yang L, Fang F, Jiao LF (2020) Electrocatalytic hydrogen evolution of ultrathin Co-Mo(5)N(6) heterojunction with interfacial electron redistribution. Energy Mater 10:2002176. https://doi.org/10.1002/aenm.202002176

[15] Xie J, Zhang J, Li S, Grote F, Zhang X, Zhang H, Wang R, Lei Y, Pan B, Xie Y (2014) Correction to controllable disorder engineering in oxygen-incorporated MoS_2 ultrathin nanosheets for efficient hydrogen evolution. J Am Chem Soc 136:1680–1680. https://doi.org/10.1021/ja4129636

[16] Zhu Y, Chen G, Xu X, Yang G, Liu M, Shao Z (2017) Enhancing electrocatalytic activity for hydrogen evolution by strongly coupled molybdenum nitride@nitrogen-doped carbon porous nano-octahedrons. ACS Catal 7:3540–3547. https://doi.org/10.1021/acscatal.7b00120

[17] Ma R, Zhou Y, Chen Y, Li P, Liu Q, Wang J (2015) Ultrafine molybdenum carbide nanoparticles composited with carbon as a highly active hydrogen-evolution electrocatalyst. Angew Chem Int Ed 54:14723–14727. https://doi.org/10.1002/anie.201506727

[18] Chen Y, Yu G, Chen W, Liu Y, Li GD, Zhu P, Tao Q, Li Q, Liu J, Shen X, Li H, Huang X, Wang D, Asefa T, Zou X (2017) Highly active, nonprecious electrocatalyst comprising borophene subunits for the hydrogen evolution reaction. J Am Chem Soc 139:12370–12373. https://doi.org/10.1021/jacs.7b06337

[19] Yang W, Tian JB, Hou LQ, Deng BJ, Wang S, Li R, Yang F, Li YF (2019) Hierarchical MoP hollow nanospheres anchored on a N, P, S-doped porous carbon matrix as efficient electrocatalysts for the hydrogen evolution reaction. Chemsuschem 12:4662–4670. https://doi.org/10.1002/cssc.201902043

[20] Wang YQ, Xie Y, Zhao L, Sui XL, Gu DM, Wang ZB (2019) Hierarchical heterostructured Mo_2C/Mo_3Co_3C bouquet-like nanowire arrays: an efficient electrocatalyst for hydrogen evolution reaction. ACS Sustain Chem Eng 7:7294–7303. https://doi.org/10.1021/acssuschemeng.9b00358

[21] Cheng ZH, Gao J, Fu Q, Li CX, Wang XP, Xiao YK, Zhao Y, Zhang ZP, Qu LT (2017) Interconnected molybdenum carbide based nanoribbons for highly efficient and ultrastable hydrogen evolution. ACS Appl Mater Interfaces 9:24608–24615. https://doi.org/10.1021/acsami.7b06329

[22] Esposito DV, Hunt ST, Kimmel YC, Chen JG (2012) A new class of electrocatalysts for hydrogen production from water electrolysis: metal monolayers supported on low-cost transition metal carbides. J Am Chem Soc 134:3025–3033. https://doi.org/10.1021/ja208656v

[23] Liu YL, Luo XH, Zhou CL, Du S, Zhen DS, Chen B, Li J, Wu Q, Iru Y, Chen DC (2020) A modulated electronic state strategy designed to integrate active HER and OER components as hybrid heterostructures for efficient overall water splitting. Appl Catal B Environ 260:118197. https://doi.org/10.1016/j.apcatb.2019.118197

[24] Zheng YR, Dong J, Huang CP, Xia LG, Wu Q, Xu QJ, Yao WF (2020) Co-doped $Mo-Mo_2C$ cocatalyst for enhanced $g-C_3N_4$ photocatalytic H_2 evolution. Appl Catal B Environ 260:118220. https://doi.org/10.1016/j.apcatb.2019.118220

[25] Hu ZH, Huang JT, Luo Y, Liu MQ, Li XB, Yan MG, Ye ZG, Chen Z, Feng ZJ, Huang SF (2019) Wrinkled Ni-doped Mo_2C coating on carbon fiber paper: an advanced electrocatalyst prepared by molten-salt method for hydrogen evolution reaction. Electrochim Acta 319:293–301. https://doi.org/10.1016/j.electacta.2019.06.178

[26] Lin HL, Zhang WB, Shi ZP, Che MW, Yu X, Tang Y, Gao QS (2017) Electrospinning hetero-nanofibers of Fe_3C-Mo_2C/nitrogen-doped-carbon as efficient electrocatalysts for hydrogen evolution. Chemsuschem 10:2597–2604. https://doi.org/10.1002/cssc.201700207

[27] Cui W, Cheng N, Liu Q, Ge C, Asiri AM, Sun X (2014) Mo_2C Nanoparticles decorated graphitic carbon sheets: biopolymer derived solid-state synthesis and application as an efficient electrocatalyst for hydrogen generation. ACS Catal 4:2658–2661. https://doi.org/10.1021/cs5005294

[28] Chen YY, Zhang Y, Jiang WJ, Zhang X, Dai Z, Wan LJ, Hu JS (2016) Pomegranatelike N, P-doped M_o2C@C nanospheres as highly active electrocatalysts for alkalinenhydrogen evolution. ACS Nano 10:8851–8860. https://doi.org/10.1021/acsnano.6b04725

[29] Liu YP, Yu GT, Li GD, Sun YH, Asefa T, Chen W, Zou XX (2015) Coupling Mo_2C with nitrogen-rich nanocarbon leads to efficient hydrogen-evolution electrocatalytic sites. Angew Chem Int Edit 54:10752. https://doi.org/10.1002/anie.201504376

[30] Fan YR, Zhao ZB, Zhou Q, Li GD, Wang XZ, Qiu JS, Gogotsi Y (2013) Nitrogen-doped carbon microfibers with porous textures. Carbon 58:128–133. https://doi.org/10.1016/j.carbon.2013.02.040

[31] Zhang SL, Zhang Y, Jiang WJ, Liu X, Xu SL, Huo RJ, Zhang FZ, Hu JS (2016) Co@N-CNTs derived from triple-role CoAl-layered double hydroxide as an efficient catalyst for oxygen reduction reaction. Carbon 107:162–170. https://doi.org/10.1016/j.carbon.2016.05.056

[32] Wu C, Li JH (2017) Unique hierarchical Mo_2C/C nanosheet hybrids as active electrocatalyst for hydrogen evolution reaction. ACS Appl Mater Interfaces 9:41314–41322. https://doi.org/10.1021/acsami.7b13822

[33] Zhang XJ, Chen YF, Wang B, Chen ML, Yu B, Wang XQ, Zhang WL, Yang DX (2019) FeNi nanoparticles embedded porous nitrogen-doped nanocarbon as efficient electrocatalyst for oxygen evolution reaction. Electrochim Acta 321:134720. https://doi.org/10.1016/j.electacta.2019.134720

[34] Guo D, Zhang HM, Yu XZ, Zhang M, Zhang P, Li QH, Wang TH (2013) Facile synthesis and excellent electrochemical properties of $CoMoO_4$ nanoplate arrays as supercapacitors. J Mater Chem A 24:7247–7254. https://doi.org/10.1039/C3TA10909G

[35] Yu L, Xiao Y, Luan CL, Yang JT, Lbw HY, Wang Y, Zhang X, Dai XP, Yang Y, Zhao HH (2013) Cobalt/molybdenum phosphide and oxide heterostructures encapsulated in N-doped carbon nanocomposite for overall water splitting in alkaline media. ACS Appl Mater Interfaces 11:6890–6899. https://doi.org/10.1021/acsami.8b15653

[36] Lu C, Huang YH, Wu YJ, Li J, Cheng JP (2018) Camellia pollen-derived carbon for supercapacitor electrode material. J Power Sources 394:9–16. https://doi.org/10.1016/j.jpowsour.2018.05.032

[37] Lin ZX, Wan WM, Yao SY, Chen JG (2018) Cobalt-modified molybdenum carbide as a selective catalyst for hydrodeoxygenation of furfural. Appl Catal B Environ 233:160–166. https://doi.org/10.1016/j.apcatb.2018.03.113

[38] Huo XD, Wang ZQ, Huang JJ, Zhang R, Fang YT (2016) Bulk Mo and Co-Mo carbides as catalysts for methanation. Catal Commun 79:39–44. https://doi.org/10.1016/j.catcom.2016.03.001

[39] Li XY, Zhang R, Luo YS, Liu Q, Lu SY, Chen G, Gao SY, Chen S, Sun XP (2020) A cobalt-phosphorus nanoparticle decorated N-doped carbon nanosheet array for efficient and durable hydrogen evolution at alkaline pH. Sustain Energy Fuels 4:3884–3887. https://doi.org/10.1039/D0SE00240B

[40] Liu TT, Liu DN, Qu FL, Wang DX, ZhangGe LRX, Hao S, Ma YJ, Du G, Asiri AM, Chen L, Sun XP (2017) Enhanced electrocatalysis for energy-efficient hydrogen production over CoP catalyst with nonelectroactive Zn as a promoter. Adv Energy Mater 7:1700020. https://doi.org/10.1002/aenm.201700020

[41] Pei Z, Xu L, Xu W (2018) Hierarchical honeycomb-like Co_3O_4 pores coating on $CoMoO_4$ nanosheets as bifunctional efficient electrocatalysts for overall water splitting. Appl Surf Sci 433:256–263. https://doi.org/10.1016/j.apsusc.2017.09.248

[42] Xiang R, Duan YJ, Peng LS, Wang Y, Tong C, Zhang L, Wei ZD (2019) Three-dimensional core@shell $Co@CoMoO_4$ nanowire arrays as efficient alkaline hydrogen evolution electrocatalysts. Appl Catal B Environ 246:41–49. https://doi.org/10.1016/j.apcatb.2019.01.035

[43] Lv JL, Guo WL, Liang TX (2016) Synthesis of $Co_3O_4@$-$CoMoO_4$ core-shell architectures nanocomposites as high-performance supercapacitor electrode. J Electroanal Chem 783:250–257. https://doi.org/10.1016/j.jelechem.2016.11.013

[44] Xu XW, Shen JF, Li N, Ye MX (2014) Microwave-assisted synthesis of graphene/$CoMoO_4$ nanocomposites with enhanced supercapacitor performance. J Alloy Compd 616:58–65. https://doi.org/10.1016/j.jallcom.2014.07.047

[45] Xiao CL, Li YB, Lu XY, Zhao C (2016) Bifunctional porous NiFe/$NiCo_2O_4$/Ni foam electrodes with triple hierarchy and double synergies for efficient whole cell water splitting. Adv Funct Mater 26:3515–3523. https://doi.org/10.1002/adfm.201505302

[46] Hou JG, Wu YZ, Cao SY, Sun YQ, Sun LC (2017) Active sites intercalated ultrathin carbon sheath on nanowire arrays as integrated core-shell architecture: highly efficient and durable electrocatalysts for overall water splitting. Small 13:1702018. https://doi.org/10.1002/smll.201702018

[47] Wang DW, Han C, Xing ZC, Li Q, Yang XR (2018) Pt-like catalytic behavior of MoNi decorated $CoMoO_3$ cuboid arrays for the hydrogen evolution reaction. J Mater Chem A 6:15558–15563. https://doi.org/10.1039/C8TA04391D

[48] Li XY, Niu ZG, Jiang J, Ai LH (2016) Cobalt nanoparticles embedded in porous N-rich carbon as an efficient bifunctional electrocatalyst for water splitting. J Mater Chem A 4:3204–3209. https://doi.org/10.1039/C6TA00223D

[49] Zhao Z, Lu W, Yang RO, Zhu HJ, Dong WD, Sun FF, Jiang Z, Lu Y, Liu T, Du H, Ding YJ (2018) Insight into the formation of $Co@Co_2C$ catalysts for direct synthesis of higher alcohols and olefins from syngas. ACS Catal 8:228–241. https://doi.org/10.1021/acscatal.7b02403

[50] Wang S, He P, Xie ZW, Jia LP, He MQ, Zhang XQ, Dong FQ, LiuZhang HHY, Li CX (2019) Tunable nanocotton-like amorphous ternary Ni-Co-B: a highly efficient catalyst for enhanced oxygen evolution reaction. Electrochim Acta 296:644–652. https://doi.org/10.1016/j.electacta.2018.11.099

[51] Zhang Y, Wang Y, Jia S, Xu HQ, Zang JB, Lu J, Xu XP (2016) A hybrid of NiMo-Mo_2C/C as non-noble metal electrocatalyst for hydrogen evolution reaction in an acidic solution. Electrochim Acta 222:747–754. https://doi.org/10.1016/j.electacta.2016.11.031

[52] Wang DZ, Guo T, Wu ZZ (2018) Hierarchical Mo_2C/C scaffolds organized by nanosheets as highly efficient electrocatalysts for hydrogen production. ACS Sustain Chem Eng 6:13995–14003. https://doi.org/10.1021/acssuschemeng.8b02469

[53] Li B, Dai F, Xiao QF, Yang L, Shen JM, Zhang CM, Cai M (2016) Nitrogen-doped activated carbon for a high energy

hybrid supercapacitor. Energy Environ Sci 9:102–106. https://doi.org/10.1039/C5EE03149D

[54] Han NN, Yang KR, Lu ZY, Li YJ, Xu WW, Gao TF, Cai Z, Zhang Y, Batista VS, Liu W, Sun XM (2018) Nitrogen-doped tungsten carbide nanoarray as an efficient bifunctional electrocatalyst for water splitting in acid. Nat Commun 9:924. https://doi.org/10.1038/s41467-018-03429-z

[55] Tang CY, Wu ZG, Wang DZ (2016) Influence of carbon on molybdenum carbide catalysts for the hydrogen evolution reaction. Chem Cat Chem 8:1961–1967. https://doi.org/10.1002/cctc.201600107

[56] Liu YP, Li QJ, Si R, Li GD, Li W, Liu DP, Wang DJ, Sun L, Zhang Y, Zou XX (2017) Coupling sub-nanometric copper clusters with quasi-amorphous cobalt sulfide yields efficient and robust electrocatalysts for water splitting reaction. Adv Mater 29:1606200. https://doi.org/10.1002/adma.201606200

[57] Xu SR, Zhao HT, Li TS, Liang J, Lu SY, Chen G, Gao SY, Asiri AM, Wu Q, Sun XP (2020) Iron-based phosphides as electrocatalysts for the hydrogen evolution reaction: recent advances and future prospects. J Mater Chem A 8:19729–19745. https://doi.org/10.1039/D0TA05628F

[58] Song YJ, Ren JT, Yuan GG, Yao YL, Liu XY, Yuan ZY (2019) Facile synthesis of Mo_2C nanoparticles on N-doped carbon nanotubes with enhanced electrocatalytic activity for hydrogen evolution and oxygen reduction reactions. J Energy Chem 38:68–77. https://doi.org/10.1016/j.jechem.2019.01.002